BL-6A, BL-15A2/2023G061

Deformation of Microlamellae in Liquid Crystal Block Copolymers Consisting of Main-Chain Type Nematic Polyester and Rubbery Segments During Reversible Contraction

Rhoji SUZUKI, Yuki IKEDA, and Masatoshi TOKITA[1]
[1] Department of Chemical Science and Technology, Tokyo Institute of Technology, Ookayama, Meguro, Tokyo 152-8550, Japan

1 Introduction

Crosslinking semiflexible liquid crystal (LC) polymers in the macroscopically aligned LC state yields monodomain LCEs (MDLCEs), which exhibit reversible morphing on the LC-to-isotropic liquid phase transition. De Gennes proposed a type of monodomain liquid crystal elastomers (MDLCE) of a triblock copolymer composed of a main-chain type nematic liquid crystal polymer (LCP) segment bonded to rubbery crosslinked amorphous segments at both ends.[1] The LCP segment isolates from the rubbery ones to form LC block lamellae, which alternatively pile up with rubbery block ones, forming a nematic LC with the nematic director orientation perpendicular to the lamellar interface. We prepared triblock copolymer LC elastomers (LCEs) composed of a main-chain LC polyester bonded to photo-crosslinked poly(2-cinnamoyloxyethyl methacrylate) at both ends.[2] This LCE had a chemical structure similar to that designed by de Gennes.[1] The copolymer film formed lamellar microdomains stacked along the LC director orientation and contracted reversibly along the director orientation on the LC isotropization by a factor of 1.1–1.2, which corresponded to changes in lamellar spacing. However, the contraction force could not be measured for enough thin films for photocrosslinking.

In this study, we designed an ABA-type triblock copolymer with a main-chain NLC polyester block bonded to cross-linkable polymethacrylate (PMA) A blocks at both ends. The copolymers, designated as BB*x*-B*r*A*y*, comprise a nematic poly(2-propoxy butyl 4,4′-biphenyl dicarboxylate) (BB) with the number average molecular weight *x* kDa bonded at both ends to poly(butyl methacrylate–*ran*–2-allyloxycarbonyloxy ethyl methacrylate) (B*r*A) blocks, where *y* denotes the weight fraction of poly(B*r*A) segment (Fig. 1a). The BB*x*-B*r*A*y* copolymer was doped with pentaerythritol tetra(3-mercaptopropionate) (PEThTMP, Fig. 1b) and melt drawn to yield a strip with the microstructure and the nematic LC oriented. Irradiation of UV light on the strip enabled the allyloxycarbonyloxy ethyl methacrylate (ACEMA) units to react with PEThTMP. As a result, the poly(B*r*A) segment crosslinked and yielded a BB*x*-B*r*A*y*-CL elastomer. The elastomer strip had an LC director lying along the lengthwise, and the BB polyester segregated from crosslinked poly(B*r*A) blocks and formed lamellar microdomains. The lamellae zigzagged transversely or were undulated along the nematic director orientation, which differed from de Gennes's design, which assumed the stacking of flat lamellae along the nematic director orientation. With the increase in temperature beyond the nematic-to-isotropic transition temperature of the BB segment, strips with one-end fixed showed reversible contraction along the lengthwise by a factor of ~1.4. We examined the deformation of the microlamellae for BB*x*-B*r*A*y*-CL during the contraction using synchrotron radiation (SR) small-angle X-ray scattering (SAXS).

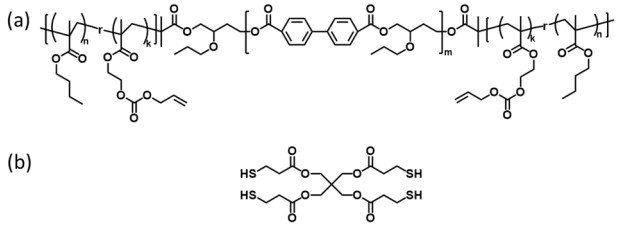

Fig. 1.: Chemical structure of (a) BB*x*-B*r*A*y* copolymer and (b) PEThTMP.

2 Experiment

Two BB*x*-B*r*A*y*-CLs of BB11-BrA36-CL and BB38-BrA27-CL were prepared and confirmed enough degree of crosslinking from the gel fraction (f_g) of 70–80%, which was the ratio of the dry mass of the insoluble part after 24 h of immersion of a film sample in chloroform to the initial weight of the sample. BB11-BrA36-CL and BB38-BrA27-CL exhibited an endothermic peak at 88 and 109°C, respectively, in the heating DSC thermogram measured at a rate of 10°C min^{-1}, attributed to the isotropization of the nematic LC formed by the BB segment.

SR-SAXS measurement was performed at the BL-6A (BL-15A2) beamline in Photon Factory, equipped with a Dectris PILATUS 1M (2M) detector with a camera length of approximately 2 (3.5) m, using an X-ray with a wavelength of 0.15 (0.20) nm. X-ray was irradiated to a sample for 60 s to measure one frame while regulating the sample temperature using a LINKAM 10002L hotstage.

Transmission electron microscopy (TEM) was performed on a Hitachi H-7650 Zero A electron microscope operating at 100 kV in bright-field mode. Samples were exposed to RuO_4 vapors at ambient temperature to stain the LC segment selectively.

Raman spectra were recorded on a JASCO NRS-5100 using the 532 nm line of Nd:YAG laser as the excitation source. The sample temperature was regulated using a LINKAM 10002L hot stage. All measurements were conducted with a backscattering configuration using a microscope with an objective 50× and an aperture 40 μm. The spectra were measured with an acquisition time of 20 s, and the fluorescence was eliminated using the JASCO software.

3 Results and Discussion

BB*x*-B*r*A*y*-CL formed microstructures with constituent segments segregated from each other, which were confirmed by TEM and SAXS (Fig. 2). The TEM image of a BB11-BrA36-CL strip displayed stripes zigzagging and transversing the strip length direction. The LC segment appeared dark due to preferential staining over the amorphous one. The first Fourier-transformed (FFT) pattern of the image exhibited four-point maxima in the inner part, which is similar to the SAXS pattern found on the right side. The TEM image of BB38-BrA27-CL displayed stripes undulating along the elongation direction. The FFT pattern revealed an ellipsoid-shaped maximum. The SAXS pattern exhibited a comparable ellipsoid-shaped scattering with four maxima along the contour. Consequently, the SAXS pattern can be attributed to the lamellae undulating along the sample lengthwise. The azimuthal direction of the maxima corresponds to the normal lamellar orientation between the peaks and valleys of the undulated lamellae. These microlamellar morphologies are similar to those reported for ABA-type LCBCPs with main-chain NLC segments as the B block.[3,4]

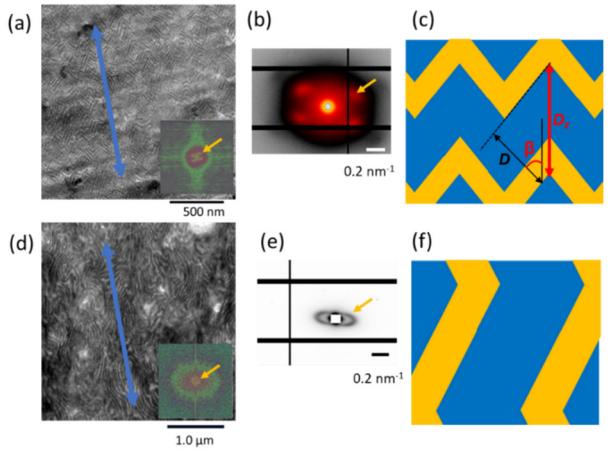

Fig. 2.: (a) TEM and (b) SAXS images and (c) schematic of the microstructure of BB11-BrA36-CL. (d), (e) and (f) reveal observations for BB38-BrA27-CL. The inset in the TEM image represents the FFT image. The blue arrow on the TEM image indicates the direction of the sample length. The SAXS patterns were measured for a sample strip with the lengthwise direction in the vertical direction. The yellow arrows in the FFT and SAXS images point to the corresponding maxima between the FFT and SAXS images. In (c), D, D_z, and β denote the lamellar spacing, lamellar spacing measured along the strip length, and folding angle of the lamellae, respectively.

When the temperature was raised past the T_i, the BB*x*-B*r*A*y*-CL strips showed contraction along the length, involving a decrease in the NLC orientational order. The degree of NLC orientation in BB*x*-B*r*A*y*-CL cannot be determined using the WAXS pattern. BB*x*-B*r*A*y*-CL overlaps scattering from the amorphous segments with scattering at $2\theta \sim 20°$ from the nematic LC, preventing estimating the degree of nematic orientation from the intensity distribution of the scattering measured along the azimuthal direction. Here, nematic orientation was measured via Raman anisotropy (R) of the peak at 1606 cm^{-1}. R was determined during the heating process, and the results were plotted against the temperature in Fig. 3. The same panel included the DSC thermogram measured for an unfixed (free) sample. The sample strips decreased the R value from 7 ($S = 0.7$) at 50°C to 1 ($S = 0$) in the broader temperature region compared with that of the endothermic DSC peak. Thus, the nematic orientation lay parallel to the strip length, which completely disappeared at $T > T_i$. The reversibility of R, i.e., the recovery of nematic order, was confirmed through measurement of the R for the strips cooled to 50 °C.

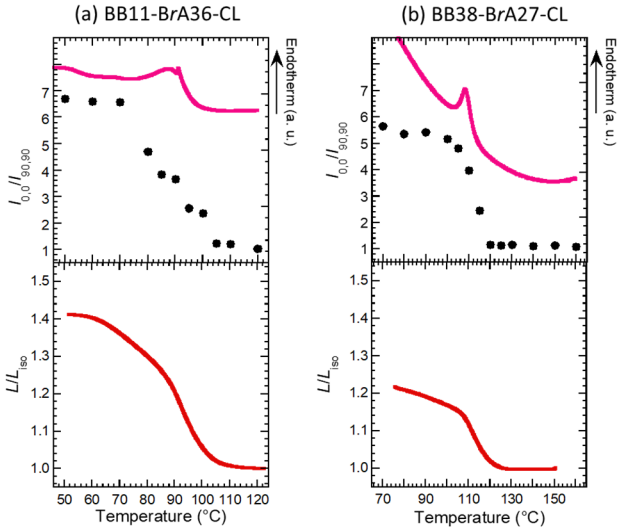

Fig. 3.: (Upper part) The dichromic ratio ($R = I_{0,0}/I_{90,90}$) of the Raman peak at 1606 cm^{-1} at the temperature measured for (a) BB11-BrA37-CL strips and (b) BB38-BrA27-CL strips plotted against temperature (closed circles). The heating DSC thermogram measured for an unfixed sample at a rate of 10°C min^{-1} is added with a solid curve. (Lower part) The strip length measured for (c) BB11-BrA37-CL strips and (d) BB38-BrA27-CL strips with the increase in the temperature at a rate of 2 °C min^{-1}.

The lower part of Fig. 3a shows the length (L) measured for a BB11-BrA36-CL strip during the heating process plotted against the values normalized to those of L_{iso} measured at $T > T_i$. The strip underwent a contraction along the length parallel to the nematic director orientation, decreasing L to 1/1.4 times the original length; this finding is comparable with human muscle contraction.[5] Similar temperature dependences of L/L_{iso} were measured for BB38-BrA27-CL strips (Fig. 3b). BB38-BrA27-CL attained a smaller retraction of 1/1.2.

The strips in the heating/cooling process were examined for the microstructure by synchrotron radiation SAXS. The SAXS measurements were conducted for a strip fixed at the upper end on a hot stage, with the longwise situated in the vertical direction and perpendicular to the X-ray beam. Due to the small space of the hot stage, the strip could not be tensed with a small load to prevent loosening, allowing the lengthwise direction at the X-ray illuminated position to change. Thus, a BB11-B*r*A36 strip showed distortion

during heating, which caused the lengthwise direction rotation on the SAXS pattern and recovered during cooling (Fig. 4a–4c). A BB38-BrA27-CL strip distortion was smaller than a BB11-BrA36 strip and presented a minor sample rotation (Fig. 4d–4f). All the strips decreased scattering intensity with the isotropization of LCs because of the minor electron density difference between the LC segment in the isotropic phase and the amorphous segment.

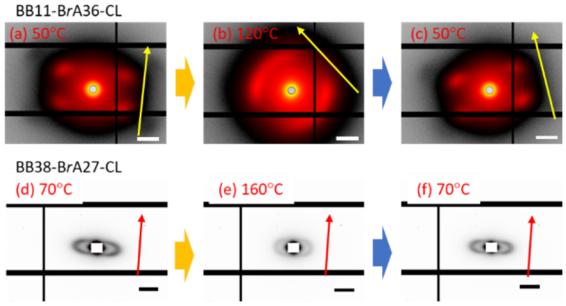

Fig. 4.: SAXS patterns of a strip of BB11-B*r*A36-CL measured during heating at (a) 50 °C and (b) 120 °C followed by cooling to (c) 50 °C. SAXS patterns of a strip of BB38-B*r*A27-CL measured during heating at (d) 70 °C and (e) 160 °C followed by cooling to (f) 70 °C. In (a)–(c), the arrow in each panel indicates the strip lengthwise.

The essential change in lamellar morphology appeared as the alteration in the azimuthal position of the scattering maximum measured from the strip lengthwise (β) and lamellar spacing (D). The values of β and D determined during the heating process were plotted against the temperature in Fig. 5. With the increase in the temperature, a BB11-BrA36-CL strip maintained a constant D at 23.8 nm while decreasing β from 58° to 35°. A BB38-BrA27-CL strip maintained a constant D at 45.5 nm while decreasing β from 76° to 62°, as measured using four intensity maxima on the ellipsoid-shaped scattering maximum. Thus, the strip caused a decrease in the folding angle of the zigzag or undulated lamellae but notably maintained a lamellar spacing.

Such a microlamellar morphology change can be related to alterations in the strip length (L). Here, L relates to the lamellar period measured along the strip lengthwise (D_z) rather than D. D_z equals $D/\cos\beta$ irrespective of the direction of lamellae zigzag or undulation, i.e., for BB11-BrA36-CL and BB38-BrA27-CL (Fig. 2c and 2f). As displayed in Fig. 5, the value of $D_z/D_{z,iso}$, where the subscript "iso" denotes that the value measured at $T > T_i$, is plotted as a function of temperature for comparison with the value of L/L_{iso}. The maximum of $D_z/D_{z,iso}$ relates well to that of L/L_{iso}. BB11-BrA36-CL had a maximum value of $D_z/D_{z,iso}$ = 1.5 at the lowest temperature, which corresponded with the maximum change in the strip length L/L_{iso} = 1.4. In contrast, BB38-BrA27-CL increased $D_z/D_{z,iso}$ to 1.4, which was more significant than the maximum value of L/L_{iso} of 1.2. A low lamellar orientation would make L/L_{iso} smaller than $D_z/D_{z,iso}$.[2] However, the tendency of $D_z/D_{z,iso}$ to decrease at a higher temperature than L/L_{iso} over experimental errors is a common observation for both elastomers. We have yet to determine the reasons for the smaller-length-scale change of the lamellar deformation after the longer-length-scale change of the strip length. SR-SAXS measurements were conducted using the same type of hot stage to control the sample temperature to the Raman spectra measurements. The temperature was scanned at a rate of 2 °C min^{-1}, the same as the sample length measurements. The change in the elastomer strip length was more associated with temperature variation of the nematic order than that of microstructure deformation.

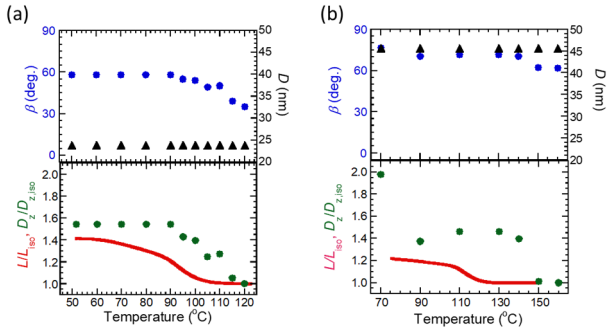

Fig. 5.: Variation in (upper part) (circles) azimuthal angle (β) of the scattering maximum measured from the sample length direction and (triangles) the lamellar spacing measured via SAXS at the temperature for (a) BB11-B*r*A36-CL and (b) BB38-B*r*A27-CL. The lower part shown includes (circles) the lamellar spacing (D_z) measured along the sample length direction and (solid line) sample strip length (L). The values of D_z and L are standardized with those of ($D_{z,iso}$ and L_{iso}, respectively) measured at the highest temperature in the measurement range.

Acknowledgment

TEM studies were performed by Mr. Jun Koki (Technical Department, Tokyo Institute of Technology), who is gratefully acknowledged. 4,4′-dimethyl biphenyl dicarboxylate was kindly supplied by Ihara Nikkei Chemical Industry Co. Ltd. The SR-SAXS measurement has been performed under the approval of the Photon Factory Program Advisory Committee (No. 23G061). This work was supported by JSPS KAKENHI Grant Number JP 19H02770 and JP23H02020.

References

[1] P.-G. de Gennes, *Comptes Rendus l'Académie Des Sci. - Ser. IIB - Mech.*, **324**, 343–348 (1997).

[2] K. Abe, M. Koga, T. Wakabayashi, S. Kang, K. Sakajiri, J. Watanabe, and M. Tokita, *Macromolecules*, **48**, 8354–8360 (2015).

[3] K. Sato, M. Koga, S. Kang, K. Sakajiri, J. Watanabe, and M. Tokita, *Macromol. Chem. Phys.*, **214**, 1089–1093 (2013).

[4] M. Koga, T. Wakabayashi, S. Kang, and M. Tokita, *Polym. J.*, **51**, 295–302 (2019).

[5] I.W. Hunter and S. Lafontaine, A comparison of muscle with artificial actuators, in: Tech. Dig. IEEE Solid-State Sens. Actuator Work., IEEE, (2017), pp. 178–185.

* tokita.m.aa@m.titech.ac.jp